



Co-doped carbon layer to lower the onset potential of hematite for solar water oxidation

Huiwen Lan¹, Yujian Xia¹, Kun Feng, Aimin Wei, Zhenhui Kang*, Jun Zhong*

Institute of Functional Nano and Soft Materials Laboratory (FUNSOM), Jiangsu Key Laboratory for Carbon-Based Functional Materials & Devices, Soochow University, Suzhou 215123, PR China



ARTICLE INFO

Keywords:

Hematite
Carbon layer
Co-doping
Low onset potential
Solar water splitting

ABSTRACT

Hematite is a promising photocatalyst for water oxidation while the practical performance of hematite has been hindered by poor conductivity and strong charge recombination. Here we report a Co-doped carbon layer on hematite to significantly enhance the solar water oxidation performance, which shows a large cathodic onset potential shift of 300 mV representing one of the largest values ever reported for hematite photoanodes. The final photocurrent at 1.23 V vs. RHE can also achieve a high value of 2.24 mA/cm². Based on synchrotron radiation X-ray absorption spectroscopy, the thin Co-doped carbon layer consists of both sp² carbon structure with good conductivity and embedded CoCO₃ (or CoO) with good OER kinetics. A thin layer itself can also block the surface defects to suppress the recombination. Thus the Co-doped carbon layer can act as a triple functional material to simultaneously improve the surface conductivity, block the surface defects, and accelerate the OER process, which can finally result in a large onset potential shift. The facile method to decorate hematite with an effective carbon layer may help for the rational design of hematite with high efficiency.

1. Introduction

Hematite is a very promising photocatalyst for water splitting since it has a favorable band gap (2.1–2.2 eV), exhibits a good stability, and is abundant in the earth with low cost [1–6]. However, in practical application the performance of hematite is highly hindered by many factors such as strong charge recombination, poor conductivity, and slow oxygen evolution reaction (OER) kinetics at the hematite/electrolyte interface [7–16]. Various methods were used to solve these problems. For example, different kinds of elemental doping were adopted to improve the conductivity [17–19]. The surface recombination can also be reduced by using passivation layers such as FeOOH, Al₂O₃, In₂O₃ and SiO₂ to block the surface defects [7–13]. Reducing of defects as well as accelerating the hole transfer could also be achieved by molecular modifications on the hematite surface [14,15,20,21]. To improve the OER kinetics, surface deposition of cocatalysts such as FeNiO_x, Co-Pt or IrO₂ were widely reported [4,2–6]. All the approaches could be combined together to form multi-components for a high performance [22,23]. However, a facile method to simultaneously overcome the problems without multiple processes is still on the way.

Carbon materials with a sp² bonding structure (such as graphene or carbon nanotube) typically show good conductivity with rich electrons,

which is expected to promote the performance of hematite [24–29]. For example, a carbon layer created in the synthesis process of hematite by the pyrolysis of ferrocene could effectively introduce oxygen vacancies and enhance the conductivity of hematite [24]. However, the reported method could only be applied to the ferrocene based hematite. Recently Wang et al. also showed the formation of carbon layer on hematite by adding various organic acid in the high temperature treatment [25,26]. The carbon layer was reported to serve as a surface passivation layer and consequently lower the onset potential [25,26]. Direct deposition of graphene layer on hematite was also reported, which could suppress the surface recombination [27]. Although the literatures have shown successful deposition of carbon layers on hematite with many advantages [24–29], unfortunately, the final performance of carbon coated hematite was still very limited (onset potential shift less than 110 mV and photocurrent less than 2.1 mA/cm² at 1.23 V vs. RHE), suggesting the urgent requirement of a good way to couple the carbon layer on hematite.

Here we report a facile method to decorate carbon layer on hematite with high efficiency by a hydrothermal process using glucose as the carbon precursor. The hydrothermal method can create a good contact between carbon layer and hematite without a significant surface reduction. Thus the carbon layer can effectively enhance the surface

* Corresponding authors.

E-mail addresses: zhkang@suda.edu.cn (Z. Kang), jzhong@suda.edu.cn (J. Zhong).

¹ These authors contributed equally to this work.

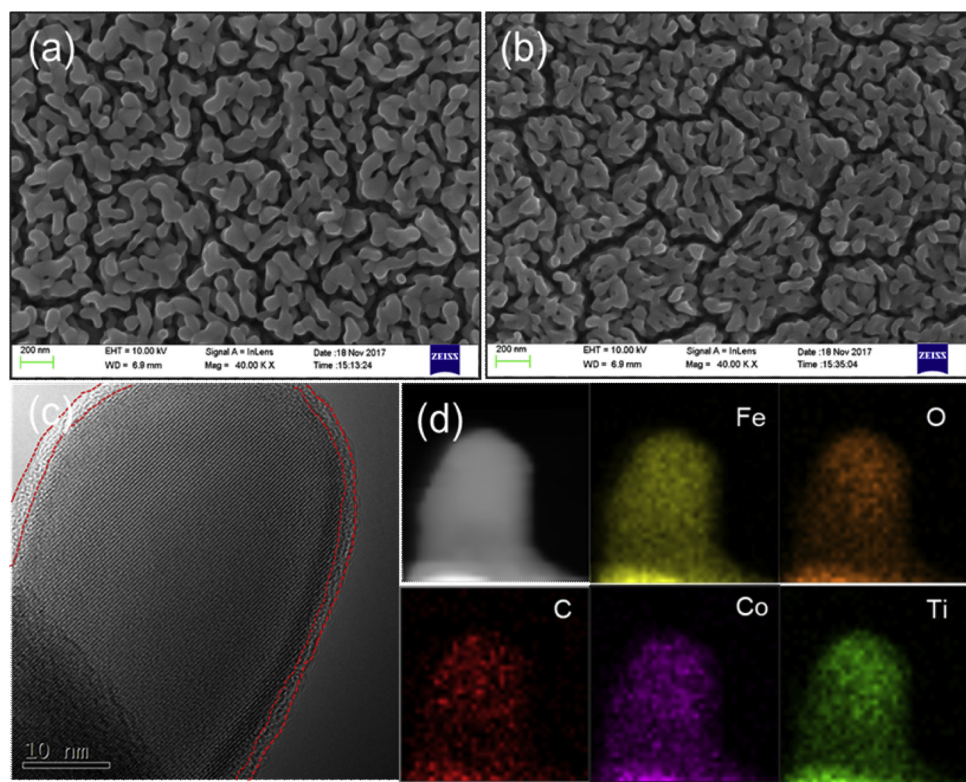


Fig. 1. (a) and (b): SEM images of Ti-Fe₂O₃ and C-Co-Ti-Fe₂O₃, respectively. (c) and (d): HRTEM image and the corresponding EDS elemental mappings of C-Co-Ti-Fe₂O₃.

conductivity of hematite and suppress the recombination, leading to a large cathodic onset potential shift of 270 mV. Moreover, when coupling Co precursor in the hydrothermal process, a Co-doped carbon layer can be introduced on hematite which can further improve the performance. Actually, for Ti-treated hematite, the Co-doped carbon layer can achieve a large cathodic onset potential shift of 300 mV, representing one of the largest values ever reported for hematite photoanodes. The enhanced photocurrent also shows a good value of 2.24 mA/cm² at 1.23 V vs. RHE. The improved performance by Co-doped carbon layer can be attributed to the enhanced surface conductivity by sp^2 carbon structure, the suppressed electron-hole recombination by a carbon layer, and the accelerated OER kinetics by Co based material. It should be noted that the single layer of Co-doped carbon can simultaneously improve the conductivity, suppress the recombination and accelerate the OER as a triple functional material, which may help for the rational design of hematite with high efficiency.

2. Experimental section

2.1. Preparation of photoanodes

The pristine hematite photoanodes were prepared on a fluorine-doped SnO₂ (FTO) glass by using a modified hydrothermal method, as reported in our previous work [3,30]. Typically, a solution of 0.1 M sodium nitrate (NaNO₃) and 0.09 M ferric chloride (FeCl₃·6H₂O) was used for the preparation. After the hydrothermal reaction at 95 °C, FeOOH could be produced on FTO. The pristine hematite (Fe₂O₃) was prepared after further sintering in air [3,30]. The synthesis process can be found in Fig. S1. Ti-modified hematite was prepared by a pre-treatment of the FTO substrate before the hydrothermal reaction [30], in which the FTO was immersed in a TiCl₄ solution. We only used the modified FTO instead of the untreated FTO for the preparation of Ti-modified hematite (Ti-Fe₂O₃) [30]. The process is also shown in Fig. S2.

To prepare C and Co treated samples, the hematite samples were

further treated by an additional hydrothermal process. In this case 70 mL aqueous solution with 3.8 mM glucose (C₆H₁₂O₆) and 0.24 mM cobalt nitrate (Co(NO₃)₂·6H₂O) was used as the reaction solution. The hematite samples in the solution were heated at 160 °C for 3 h. Then the final products were marked as C-Co-Fe₂O₃ or C-Co-Ti-Fe₂O₃, respectively. To prepare the samples with only C or only Co, we only changed the solution in the autoclave with only C or only Co precursor, respectively.

2.2. Structural characterization

The hematite morphology was probed by Transmission Electron Microscopy (TEM). The hematite nanorods were scratched from the FTO substrate for the TEM experiments. Then the hematite powder was well dispersed in the ethanol solution by sonication. The above solution was loaded on the copper mesh through drop-coating and dried at room temperature for 3 h for TEM experiments. Scanning Electron Microscope (SEM) was also used for the morphology characterization (FEI Quanta 200 F). X-ray photoelectron Spectrometer (XPS) and X-ray Diffraction (XRD) experiments were performed to investigate the structural information. X-ray absorption spectroscopy (XAS) experiments in the soft X-ray range were performed at the XMCD beamline at National Synchrotron Radiation Laboratory (NSRL), the Soft X-ray beamline at Beijing Synchrotron Radiation Facility (BSRF) and the 08U beamline at Shanghai Synchrotron Radiation Facility (SSRF).

2.3. PEC measurements

The working area of the photoanode was around 0.1 cm². We used an electrochemical workstation (the CHI 660D type) to measure the PEC performance. The electrolyte (1 M NaOH) exhibited a pH value of 13.6. We used the potential vs. reversible hydrogen electrode (RHE) in this work by a conversion of the measured voltage. The potential was scanned at a rate of 50 mV/s. We used a Xenon High Brightness Cold

Light Source with AM 1.5 filter to simulate the sunlight with a normal power density of 100 mW/cm^2 . a Xenon lamp was used to collect the incident photon-to-current conversion efficiencies (IPCE) data [30].

3. Results and discussion

3.1. Characterization of catalysts

The preparation processes of C-Co- Fe_2O_3 and C-Co-Ti- Fe_2O_3 can be found in Figs. S1 and S2, respectively. An additional hydrothermal process is used to decorate the Co-doped carbon layer on hematite with good contact and weak reduction. Fig. 1 shows the SEM and high-resolution TEM (HRTEM) images of the Ti- Fe_2O_3 samples with or without the C and Co treatment. The corresponding elemental mappings are also shown. From the SEM images, a nanorod structure of the samples can be observed in good agreement with the literatures [3,30]. There is no obvious morphology change after the treatment, indicating a mild surface modification. Similar SEM images of Fe_2O_3 and C-Co- Fe_2O_3 can also be found in Fig. S3. However, from the HRTEM image in Fig. 1c, a clear carbon layer (dash lines, about 2 nm thick) on hematite can be observed. The existence of C, Co, and Ti elements in the C-Co-Ti- Fe_2O_3 sample can also be confirmed by the EDS elemental mappings (Fig. 1d). The TEM images strongly confirm the successful modification of a Co-doped carbon layer on the hematite nanorods. The existence of a Co-doped carbon layer on hematite for C-Co- Fe_2O_3 is also confirmed by the HRTEM images and the corresponding elemental mappings in Fig. S4. HRTEM images and the corresponding elemental mappings of Ti- Fe_2O_3 are also presented in Fig. S5 for comparison, while no coating layer can be observed without the C and Co treatment.

XRD spectra of Fe_2O_3 , C-Co- Fe_2O_3 and C-Co-Ti- Fe_2O_3 are shown in Fig. S6, which are similar to the normal hematite structure (JCPDS 33-0664). There is no new XRD peaks. The Ti-treatment in Ti- Fe_2O_3 and C-Co-Ti- Fe_2O_3 are also studied by the Ti *L*-edge X-ray absorption spectroscopy (XAS). Ti based treatments on hematite were widely reported and typically Fe_2TiO_5 could form in hematite to enhance the hole transport [22,30–32]. Fe_2TiO_5 layer on hematite can be observed in some literatures [9,22]. However, by using our preparation method, typically it is molecular Fe_2TiO_5 modification and no Fe_2TiO_5 layer can be observed [30,31]. Here the Ti-based treatment just followed the same method used in our previous work [30]. A bulk Fe_2TiO_5 -incorporation in Ti- Fe_2O_3 can thus be created to enhance the performance [30]. The XAS data in Fig. S7 strongly confirms the formation of Fe_2TiO_5 in Ti- Fe_2O_3 [30,31].

3.2. PEC performance

The photocurrent density versus applied potential (*J-V*) curves of various hematite samples can be observed in Fig. 2. The *J-V* curves of Fe_2O_3 , Ti- Fe_2O_3 and C-Co- Fe_2O_3 are presented in Fig. 2a. Compared to the original hematite, the Ti-modified sample shows an enhanced photocurrent but exhibits a worse onset potential consistent with the literatures [30–32]. After the C and Co treatment, the C-Co- Fe_2O_3 sample exhibits a significantly enhanced performance, showing both an enhanced photocurrent and a substantial cathodic onset potential shift (with a large shift value of 210 mV). The photocurrent of C-Co- Fe_2O_3 shows significant improvement from 0.88 mA/cm^2 (Fe_2O_3) to 1.68 mA/cm^2 at 1.23 V vs. RHE. The large enhancement can be attributed to the C and Co based treatment. Moreover, when we apply the C and Co based treatment to the Ti-treated sample as shown in Fig. 2b, an obvious improvement of the performance can be observed. The sample after C and Co based treatment (C-Co-Ti- Fe_2O_3) shows a large cathodic onset potential shift with a comparison to the original Ti- Fe_2O_3 sample, which is as large as 300 mV (from 1.0 to 0.7 V vs. RHE, the onset potential shift was calculated by using the potential at the intersection point of the tangent at maximum slop of photocurrent and the dark current) [14]. To the best of our knowledge, it represents one of the

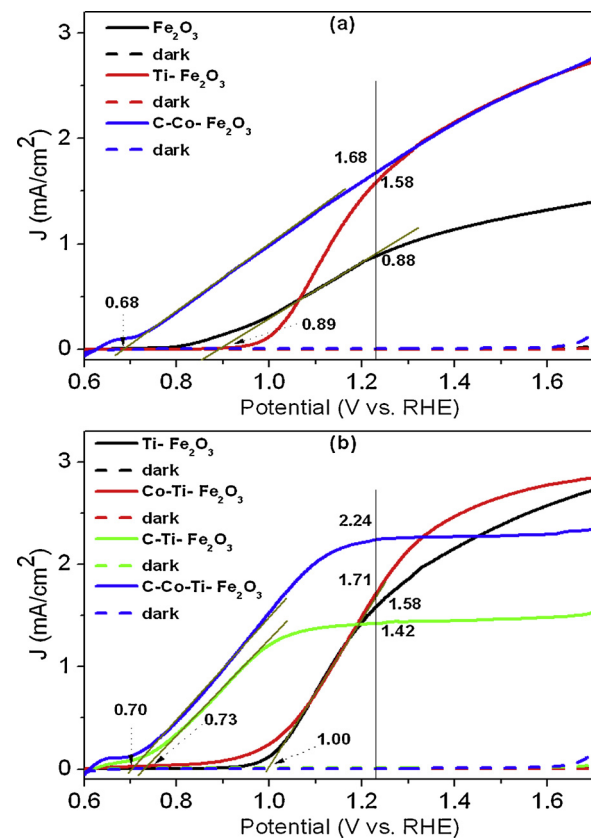


Fig. 2. (a) *J-V* scans of Fe_2O_3 , Ti- Fe_2O_3 and C-Co- Fe_2O_3 . (b) *J-V* scans of Ti- Fe_2O_3 , Co-Ti- Fe_2O_3 , C-Ti- Fe_2O_3 and C-Co-Ti- Fe_2O_3 .

largest values ever reported for the hematite photoanodes [20,22,23,33]. Interestingly, the onset potential shift shows a good shape (a parallel shift), strongly improving the photocurrents between 0.8 and 1.23 V vs. RHE. Finally we can obtain a high photocurrent value of 2.24 mA/cm^2 at 1.23 V vs. RHE.

We also show the curves of Ti- Fe_2O_3 samples after only C or only Co treatment in Fig. 2b for comparison. It shows that the C treatment can significantly lower the onset potential while the pure Co treatment can slightly enhance the photocurrent. The excellent effect of C treatment to enhance the performance can be partly attributed to its high conductivity, which can accelerate the electron transfer and reduce the recombination. Moreover, the carbon layer observed from Fig. 1 can also act as the passivation layer to block the surface defects. The facile hydrothermal treatment leads to an excellent contact between carbon layer and hematite eliminating the conventional high temperature treatment [25,26]. Typically, a direct deposition of carbon on hematite cannot create a good contact between hematite and the carbon layer. The normal way to form a good contact requires a high-temperature thermal treatment [25,26]. However, the high temperature annealing with carbon can easily induce a reduction of hematite leading to large amounts of Fe_3O_4 , which shows no photoelectrical activity [34]. The present hydrothermal method without the need of high temperature annealing perfectly solves these problems. In addition, the carbon layer is also an excellent supporting material to anchor different compositions with abundant surface groups [35,36]. Co based materials are considered as an excellent OER cocatalyst to enhance the performance of hematite [4,5,37]. However, pure Co NPs are not easy to be anchored on the smooth surface of hematite. The carbon layer can help to anchor the Co based cocatalyst. Thus the C and Co treated sample can achieve an excellent efficiency with large cathodic onset potential shift.

Fig. S8 shows the IPCE values of Fe_2O_3 , C-Co- Fe_2O_3 and C-Co-Ti- Fe_2O_3 (at 1.23 V vs. RHE), which are consistent with the *J-V* scans. At

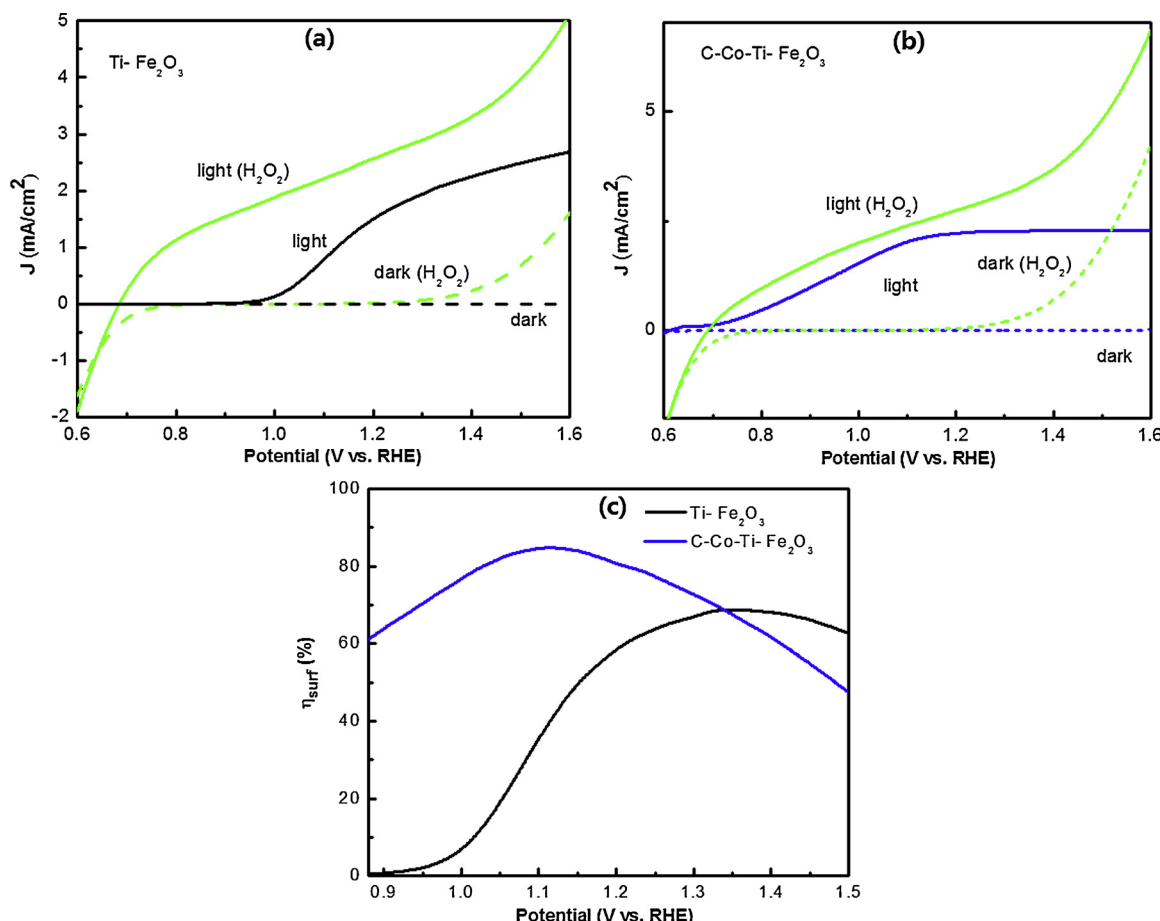


Fig. 3. J - V scans of the Ti- Fe_2O_3 (a) and C-Co-Ti- Fe_2O_3 photoanodes (b) with (green) and without H_2O_2 (0.5 M) (black or blue). (c) Calculated charge separation efficiencies (η_{surf}) of the Ti- Fe_2O_3 and C-Co-Ti- Fe_2O_3 photoanodes (For interpretation of the references to colour in this figure legend, the reader is referred to the web version of this article).

about 370 nm, C-Co-Ti- Fe_2O_3 shows the highest IPCE value of 40%. Fig. S9 shows the stability curve of C-Co-Ti- Fe_2O_3 measured at 1.23 V vs. RHE, which exhibits almost no decay in 2 h suggesting a good stability. The experimental condition of the C and Co treatment was also optimized with various C:Co ratios (the precursor ratio). The results are shown in Fig. S10, which suggests that the best C:Co ratio is 70:1.

3.3. Research on catalytic mechanism

The working mechanism is studied by using various techniques. Mott-Schottky plots of Fe_2O_3 , C-Co- Fe_2O_3 and C-Co-Ti- Fe_2O_3 are shown in Fig. S11. From the corresponding slopes in Fig. S11, the carrier densities can thus be calculated [34]. The carrier density for the pristine Fe_2O_3 is $1.15 \times 10^{20} \text{ cm}^{-3}$. For C-Co- Fe_2O_3 and C-Co-Ti- Fe_2O_3 , the carrier densities are $4.15 \times 10^{20} \text{ cm}^{-3}$ and $2.49 \times 10^{20} \text{ cm}^{-3}$, respectively. The values for the C and Co treated sample are similar to that for Fe_2O_3 , indicating no significant carrier density change. The results suggest that the treatment is not a bulk modification to increase the charge density.

The surface charge separation efficiencies of Ti- Fe_2O_3 and C-Co-Ti- Fe_2O_3 are also evaluated and the results are shown in Fig. 3. Typically, H_2O_2 (0.5 M) with high reactivity is used as a hole scavenger and the surface charge separation of H_2O_2 oxidation can be considered as a complete process (100%) [13,20]. By comparing the photocurrent values in H_2O_2 ($J_{\text{H}_2\text{O}_2}$) with that in water ($J_{\text{H}_2\text{O}}$), the calculated surface charge separation efficiency (η_{surf}) of hematite in water can thus be obtained [13,20]. There is also an equation to describe the relationship: $\eta_{\text{surf}} = J_{\text{H}_2\text{O}}/J_{\text{H}_2\text{O}_2}$. The comparison of J - V scans for Ti- Fe_2O_3 with

(green) and without (black) H_2O_2 is shown in Fig. 3a and the curves for C-Co-Ti- Fe_2O_3 are shown in Fig. 3b. At a relatively low onset potential, the photocurrent value of C-Co-Ti- Fe_2O_3 is very similar to that with H_2O_2 , indicating a high charge separation efficiency. The corresponding surface charge separation efficiencies (η_{surf}) of Ti- Fe_2O_3 and C-Co-Ti- Fe_2O_3 are shown in Fig. 3c. Obviously, the sample after C and Co treatment shows an enhanced efficiency when compared to the Ti- Fe_2O_3 sample, confirming the enhanced interface charge separation. It could be assigned to the faster charge transfer at the surface and the suppressed charge recombination with the Co-doped carbon layer [13,20]. Thus the onset potential can be obviously lowered. It is shown that the highest charge separation efficiency occurs at a potential before 1.23 V vs. RHE, which can be attributed to large onset potential shift by the C and Co treatment.

XPS data are shown in Fig. S12 to probe the electronic structure of C-Co-Ti- Fe_2O_3 . Fig. S12a shows the XPS survey scan of C-Co-Ti- Fe_2O_3 . Clear Fe and O peaks can be found indicating the typical Fe_2O_3 structure [3,30]. The peak for Sn can also be found suggesting the Sn diffusion on FTO [3,30]. Ti, C and Co signals can also be observed confirming the compositions. From the XAS spectrum in Fig. S7 the Ti component in the sample is revealed to be Fe_2TiO_5 . The XPS spectra at the Fe 2p, Co 2p and C 1s edges are also shown in Fig. S12b-d, respectively. No obvious Fe^{2+} signal can be observed in Fig. S12b, indicating no significant surface reduction after the C and Co treatment. Co signal in Fig. S12c shows an energy position similar to Co^{2+} , while the C signal in Fig. S12d shows a chemical state similar to the sp^2 carbon structure with oxidized groups.

The electronic structure of the Co doped carbon layer has been

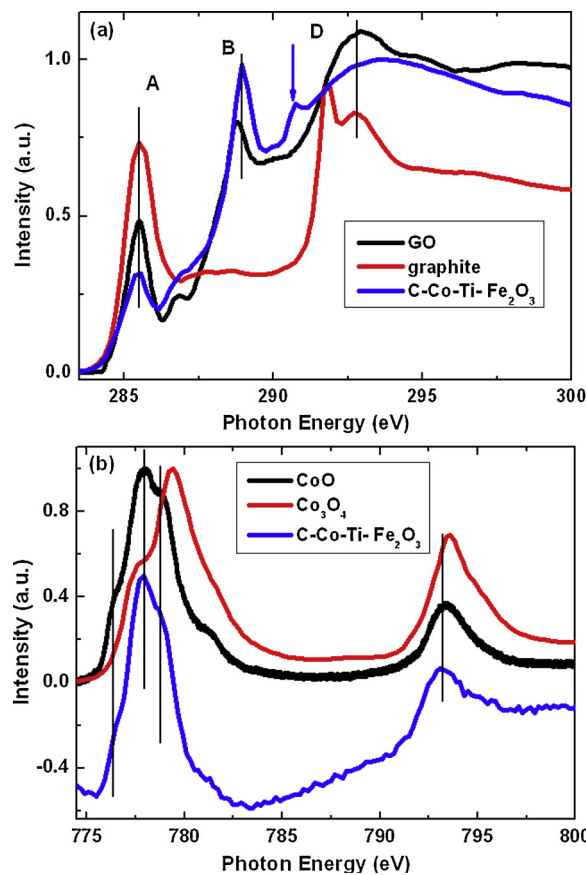


Fig. 4. XAS spectra of C-Co-Ti-Fe₂O₃ and some reference samples at the C K-edge (a) and the Co L-edge (b).

further studied by using the synchrotron radiation based XAS. The XAS spectra of C-Co-Ti-Fe₂O₃ and some reference samples at the C K-edge and the Co L-edge are shown in Fig. 4a and b, respectively. For the

graphite sample with a sp² carbon structure, the C K-edge XAS spectrum in Fig. 4a shows two main features marked as A (285.4 eV) and D (around 291.7 eV), which are typically attributed to the π^* and σ^* excitation states from the carbon ring structure, respectively [35,36,38]. Graphene oxide (GO) also shows the two features A and D for sp² carbon structure. However, the feature D for GO is broader and the feature B for GO is stronger, revealing the heavily oxidized state [35,36,38]. The strong feature B can be assigned to the oxidation of carbon with groups such as C=O and COOH [35,36,38]. Compared to GO, the C-Co-Ti-Fe₂O₃ sample also shows an obvious feature A indicating the existence of sp² carbon structure. An obvious feature B and a broad feature D can also be clearly found suggesting the oxidized structure. Thus the carbon layer on hematite can be assigned to the presence of sp² carbon with oxidized groups similar to GO. Moreover, from the XAS spectrum in Fig. 4a an additional feature at about 290.5 eV (arrow) can be observed for C-Co-Ti-Fe₂O₃, indicating the presence of CO₃²⁻ and the formation of CoCO₃ in the carbon layer [35,39].

Further evidence of the formation of CoCO₃ can be observed at the Co L-edge in Fig. 4b. Compared to the reference samples, the Co element in C-Co-Ti-Fe₂O₃ shows a chemical state similar to CoO. Combined with the presence of CO₃²⁻ in the C XAS spectrum, the Co composition can thus be assigned to CoCO₃ in the carbon layer. Also the CoO composition in the carbon layer cannot be excluded [40]. Data are also consistent with the XPS results. Thus the sp² carbon layer can accelerate the electron transport and block the defects, while the CoCO₃ (or CoO) in the carbon layer can improve the OER kinetics to synergistically enhance the performance. It should be noted that when a carbon layer was produced on Ti-Fe₂O₃, a terrace after 1.1 V vs. RHE for C-Ti-Fe₂O₃ and C-Co-Ti-Fe₂O₃ could also be observed. The rate-determining interfacial hole transfer mechanism of Ti-Fe₂O₃ could be changed after the formation of a carbon coating layer, which might partly lead to a concerted proton-electron transfer process and then result in the terrace [41]. We also measured the faradaic efficiency of C-Co-Ti-Fe₂O₃ at 1.23 V vs. RHE and presented the results in Fig. S13. By using a gas chromatography (GC), only O₂ gas can be observed from the C-Co-Ti-Fe₂O₃ photoanode without any CO composition for possible carbon gasification. The faradaic efficiency to produce O₂ is also a high

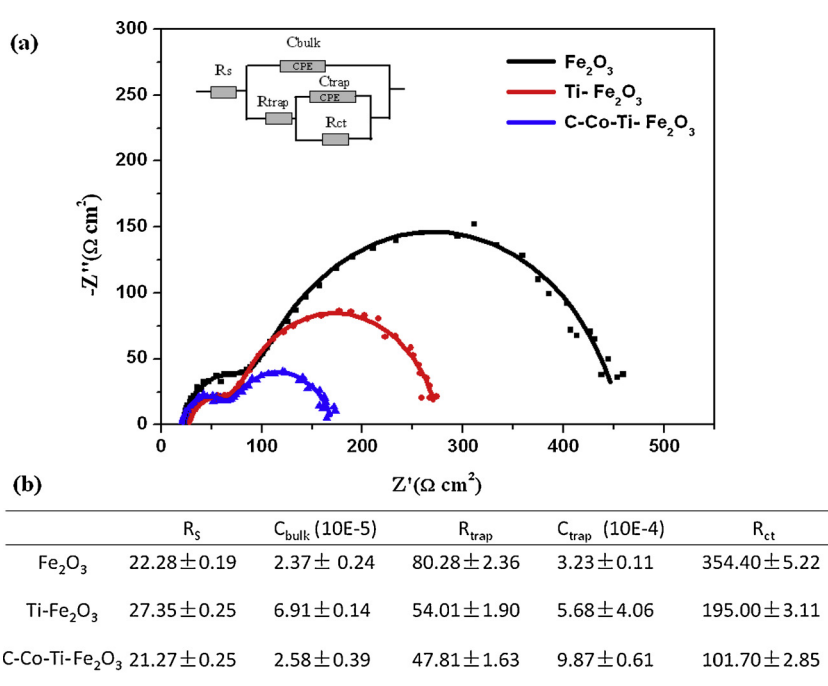


Fig. 5. (a) EIS curves of Fe₂O₃, Ti-Fe₂O₃, and C-Co-Ti-Fe₂O₃ measured at 1.23 V vs. RHE in 1 M NaOH electrolyte under the light illumination. The equivalent circuit is shown in the inset. (b) Parameters of equivalent circuit elements.

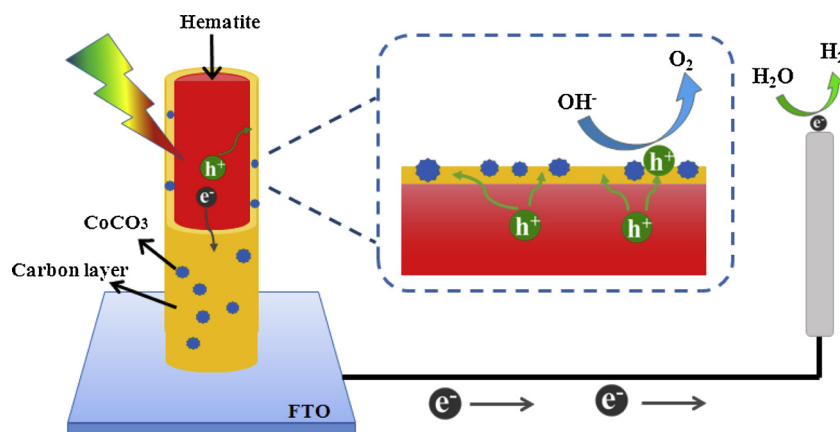


Fig. 6. Working mechanism illustration of C-Co-Ti-Fe₂O₃.

value of around 83% in Fig. S13, suggesting that the photocurrent is mainly for solar water oxidation process.

The C-Co-Ti-Fe₂O₃ sample is also studied by the electrochemical impedance spectroscopy (EIS) under the light illumination. The Nyquist plots of Fe₂O₃, Ti-Fe₂O₃, and C-Co-Ti-Fe₂O₃ measured at 1.23 V vs. RHE have been shown in Fig. 5a with the equivalent circuit (EC) in the inset [42]. Fig. 5b presents the fitting parameters of EC. Two arcs in the EIS spectra can be observed for all three samples. Typically, a smaller diameter of the arc stands for the faster charge transfer kinetics at the electrode interface [42]. Obviously, the C-Co-Ti-Fe₂O₃ sample shows the smallest diameter in Fig. 5a, revealing the best charge transfer efficiency with a Co-doped carbon layer. The fitting parameter R_{ct} (resistance for the interfacial charge transfer) for C-Co-Ti-Fe₂O₃ in Fig. 5b is also much lower than the samples without the Co-doped carbon layer, confirming the improved interface charge transfer [42]. The C-Co-Ti-Fe₂O₃ sample also exhibits a high C_{trap} value, which suggests more active surface sites [42]. The Co-doped carbon layer can act as both a passivation layer and an effective surface cocatalyst to increase the active surface states for enhanced performance [9,20,22,42,43]. The passivation layer can reduce the iron species (defect sites) and then increase the active surface states [42]. The surface cocatalysts can facilitate the OER reaction and then create more active surface states [20,43]. Thus here the increased C_{trap} for C-Co-Ti-Fe₂O₃ can be attributed to both the carbon passivation layer and the Co based surface cocatalysts to increase the surface states. The EIS data is also consistent with the PEC performance in Fig. 2. The EIS analysis at different potentials (0.8 and 0.9 V vs. RHE) are also shown in Figs. S14 and S15, respectively. The results confirm that the Co-doped carbon layer can act as both a passivation layer and an effective surface cocatalyst to improve the PEC performance.

The structure and working mechanism of C-Co-Ti-Fe₂O₃ can thus be illustrated in Fig. 6 based on the above results. In the hydrothermal process a Co-doped carbon layer can uniformly deposited on the hematite surface. The layer is mainly sp^2 carbon with oxidized groups to anchor CoCO₃ (or CoO) in the layer. The carbon layer can accelerate the surface electron transfer and block the surface defects to reduce the electron-hole recombination. Moreover, the CoCO₃ (or CoO) in the layer can act as a good cocatalyst to facilitate the OER kinetics. Thus the single layer can act as a triple functional material to significantly improve the hematite performance for solar water oxidation. An excellent performance with remarkable cathodic onset potential shift can thus be achieved. The facile treatment and the effective improvement may help for the rational design of hematite with high efficiency for the practical water splitting application.

4. Conclusion

We reported a hydrothermal decoration of carbon layer on hematite

by using glucose as the carbon precursor. The facile method can produce a good contact between carbon layer and hematite without strong reduction. The carbon layer can thus enhance the surface conductivity and reduce the electron-hole recombination by block the surface states, leading to a significant cathodic onset potential shift of 270 mV. Moreover, when adding Co precursor in the hydrothermal process, Co-doped carbon layer can be produced on hematite leading to an obvious enhancement of the performance. Especially, for Ti-treated hematite, the Co-doped carbon layer leads to a large cathodic onset potential shift of 300 mV representing one of the largest values ever reported for hematite photoanodes. The final onset potential can be a low value of 0.7 V vs. RHE. A high photocurrent of 2.24 mA/cm² at 1.23 V vs. RHE can also be obtained. The improved performance by Co-doped carbon layer can be attributed to the enhanced surface conductivity by sp^2 carbon structure, the suppressed electron-hole recombination by a carbon layer, and the accelerated OER kinetics by the embedded CoCO₃ (or CoO). The Co-doped carbon layer can act as a triple functional coating material and may help for the rational design of hematite with high efficiency.

Declaration of Competing Interest

The authors declare that they have no known competing financial interests or personal relationships that could have appeared to influence the work reported in this paper.

Acknowledgements

We acknowledge the support from NSRL, BSRF and SSRF for the XAS experiments. We acknowledge the support from Users with Excellence Program of Hefei Science Center CAS (2019HSC-UE002). This work is supported by the National Natural Science Foundation of China (U1732110). This is also a project supported by Collaborative Innovation Center of Suzhou Nano Science & Technology, Soochow University-Western University Centre for Synchrotron Radiation Research, the Priority Academic Program Development of Jiangsu Higher Education Institutions (PAPD) and the Fund for Innovative Research Teams of Jiangsu Higher Education Institutions.

Appendix A. Supplementary data

Supplementary material related to this article can be found, in the online version, at doi:<https://doi.org/10.1016/j.apcatb.2019.117962>.

References

- [1] K. Sivula, F. Le Formal, M. Grätzel, Solar water splitting: progress using hematite (α -Fe₂O₃) photoelectrodes, *ChemSusChem* 4 (2011) 432–449, <https://doi.org/10.1002/cssc.201002211>.

1002/cssc.201000416.

[2] J.Y. Kim, J.W. Jang, D.H. Youn, G. Magesh, J.S. Lee, A stable and efficient hematite photoanode in a neutral electrolyte for solar water splitting: towards stability engineering, *Adv. Energy Mater.* 4 (2014) 1400476, <https://doi.org/10.1002/aenm.201400476>.

[3] Y. Ling, G. Wang, D.A. Wheeler, J.Z. Zhang, Y. Li, Sn-doped hematite nanostructures for photoelectrochemical water splitting, *Nano Lett.* 11 (2011) 2119–2125, <https://doi.org/10.1021/nl200708y>.

[4] S.D. Tilley, M. Cornuz, K. Sivula, M. Grätzel, Light-induced water splitting with hematite: Improved nanostructure and iridium oxide catalysis, *Angew. Chem. Int. Ed.* 49 (2010) 6405–6408, <https://doi.org/10.1002/anie.201003110>.

[5] D.K. Zhong, M. Cornuz, K. Sivula, M. Grätzel, D.R. Gamelin, Photo-assisted electrodeposition of cobalt-phosphate (Co-Pi) catalyst on hematite photoanodes for solar water oxidation, *Energy Environ. Sci.* 4 (2011) 1759–1764, <https://doi.org/10.1039/c1ee01034d>.

[6] C.G. Morales-Guio, M.T. Mayer, A. Yella, S.D. Tilley, M. Grätzel, X. Hu, An optically transparent iron nickel oxide catalyst for solar water splitting, *J. Am. Chem. Soc.* 137 (2015) 9927–9936, <https://doi.org/10.1021/jacs.5b05544>.

[7] B. Iandolo, B. Wickman, I. Zorić, A. Hellman, The rise of hematite: origin and strategies to reduce the high onset potential for the oxygen evolution reaction, *J. Mater. Chem. A* 3 (2015) 16896–16912, <https://doi.org/10.1039/c5ta03362d>.

[8] R. Liu, Z. Zheng, J. Spurgeon, X. Yang, Enhanced photoelectrochemical water-splitting performance of semiconductors by surface passivation layers, *Energy Environ. Sci.* 7 (2014) 2504–2517, <https://doi.org/10.1039/c5ee01679g>.

[9] D. Monllor-Satoca, M. Bärtsch, C. Fábrega, A. Genç, S. Reinhard, T. Andreu, J. Arbiol, M. Niederberger, J.R. Morante, What do you do, titanium? Insight into the role of titanium oxide as a water oxidation promoter in hematite-based photoanodes, *Energy Environ. Sci.* 8 (2015) 3242–3254, <https://doi.org/10.1002/anie.201306263>.

[10] J.W. Jang, C. Du, Y. Ye, Y. Lin, X. Yao, J. Thorne, E. Liu, G. McMahon, J. Zhu, A. Javey, J. Guo, D. Wang, Enabling unassisted solar water splitting by iron oxide and silicon, *Nat. Commun.* 6 (2015) 7447–7452, <https://doi.org/10.1038/ncomms8447>.

[11] S. Kment, F. Riboni, S. Pausova, L. Wang, L. Wang, H. Han, Z. Hubicka, J. Krysa, P. Schmuki, R. Zboril, Photoanodes based on TiO₂ and α -Fe₂O₃ for solar water splitting—superior role of 1D nanoarchitectures and of combined heterostructures, *Chem. Soc. Rev.* 46 (2017) 3716–3769, <https://doi.org/10.1039/c6cs00015k>.

[12] H.J. Ahn, K.Y. Yoon, M.J. Kwak, J.H. Jang, A titanium-doped SiO_x passivation layer for greatly enhanced performance of a hematite-based photoelectrochemical system, *Angew. Chem. Int. Ed.* 55 (2016) 9922–9926, <https://doi.org/10.1002/anie.201603666>.

[13] J.Y. Kim, D.H. Youn, K. Kang, J.S. Lee, Highly conformal deposition of an ultrathin FeOOH layer on a hematite nanostructure for efficient solar water splitting, *Angew. Chem. Int. Ed.* 55 (2016) 10854–10858, <https://doi.org/10.1002/anie.201605924>.

[14] D. Cao, W. Luo, J. Feng, X. Zhao, Z. Li, Z. Zou, Cathodic shift of onset potential for water oxidation on a Ti⁴⁺ doped Fe₂O₃ photoanode by suppressing the back reaction, *Energy Environ. Sci.* 7 (2014) 752–759, <https://doi.org/10.1039/c3ee42722f>.

[15] Y. Yang, M. Forster, Y. Ling, G. Wang, T. Zhai, Y. Tong, A.J. Cowan, Y. Li, Acid treatment enables suppression of electron-hole recombination in hematite for photoelectrochemical water splitting, *Angew. Chem. Int. Ed.* 55 (2016) 3403–3407, <https://doi.org/10.1002/anie.201510869>.

[16] F. Le Formal, N. Tétreault, M. Cornuz, T. Moehl, M. Grätzel, K. Sivula, Passivating surface states on water splitting hematite photoanodes with alumina overlayers, *Chem. Sci.* 2 (2011) 737–743, <https://doi.org/10.1039/c0sc00578a>.

[17] C.X. Kronawitter, I. Zegkinoglou, S.H. Shen, P. Liao, I.S. Cho, O. Zandi, Y.S. Liu, K. Lashgari, G. Westin, J.H. Guo, F.J. Himpel, E.A. Carter, X.L. Zheng, T.W. Hamann, B.E. Koel, S.S. Mao, L. Vayssières, Titanium incorporation into hematite photoelectrodes: theoretical considerations and experimental observations, *Energy Environ. Sci.* 7 (2014) 3100–3121, <https://doi.org/10.1039/c4ee01066c>.

[18] Y. Zhang, S. Jiang, W. Song, P. Zhou, H. Ji, W. Ma, W. Hao, C. Chen, J. Zhao, Nonmetal P-doped hematite photoanode with enhanced electron mobility and high water oxidation activity, *Energy Environ. Sci.* 8 (2015) 1231–1236, <https://doi.org/10.1039/c4ee03803g>.

[19] S. Shen, J. Jiang, P. Guo, C.X. Kronawitter, S.S. Mao, L. Guo, Effect of Cr doping on the photoelectrochemical performance of hematite nanorod photoanodes, *Nano Energy* 1 (2012) 732–741, <https://doi.org/10.1016/j.nanoen.2012.05.013>.

[20] J. Deng, X. Lv, K. Nie, X. Lv, X. Sun, J. Zhong, Lowering the onset potential of Fe₂TiO₅/Fe₂O₃ photoanodes by interface structures: F- and Rh-based treatments, *ACS Catal.* 7 (2017) 4062–4069, <https://doi.org/10.1021/acscatal.7b00913>.

[21] H. Lan, A. Wei, H. Zheng, X. Sun, J. Zhong, Boron-passivated surface Fe^(iv) defects in hematite for highly efficient water oxidation, *Nanoscale* 10 (2018) 7033–7039, <https://doi.org/10.1039/c8nr01228h>.

[22] P. Tang, H. Xie, C. Ros, L. Han, M. Biset-Peiró, Y. He, W. Kramer, A.P. Rodríguez, E. Saucedo, J.R. Galán-Mascarós, T. Andreu, J.R. Morante, J. Arbiol, Enhanced photoelectrochemical water splitting of hematite multilayer nanowire photoanodes by tuning the surface state via bottom-up interfacial engineering, *Energy Environ.*

Sci. 10 (2017) 2124–2136, <https://doi.org/10.1039/c7ee01475a>.

[23] I.S. Cho, H.S. Han, M. Logar, J. Park, X. Zheng, Enhancing low-bias performance of hematite photoanodes for solar water splitting by simultaneous reduction of bulk, interface, and surface recombination pathways, *Adv. Energy Mater.* 6 (2016) 1501840, <https://doi.org/10.1002/aenm.201501840>.

[24] J. Deng, X. Lv, J. Gao, A. Pu, M. Li, X. Sun, J. Zhong, Facile synthesis of carbon-coated hematite nanostructures for solar water splitting, *Energy Environ. Sci.* 6 (2013) 1965–1970, <https://doi.org/10.1039/c3ee00066d>.

[25] T.H. Wang, C.C. Chiang, Y.L. Wu, C. Lin, Y.J. Cheng, Y.K. Hsieh, C.F. Wang, C.P. Huang, Characteristics of elemental carbon overlayers over hematite electrodes prepared by electrodeposition with organic acid additives, *Appl. Catal. B-Environ.* 207 (2017) 1–8, <https://doi.org/10.1016/j.apcatb.2017.02.003>.

[26] T.H. Wang, Y.N. Chen, C.C. Chiang, Y.K. Hsieh, P.C. Li, C.F. Wang, Carbon-coated hematite electrodes with enhanced photoelectrochemical performance obtained through an electrodeposition method with a citric acid additive, *ChemElectroChem* 3 (2016) 966–975, <https://doi.org/10.1002/celec.201600060>.

[27] M.P. Cardona, M. Li, W. Li, J. McCall, D. Wang, Y. Li, C. Yang, The role of graphene as an overlayer on nanostructured hematite photoanodes for improved solar water oxidation, *Mater. Today Energy* 8 (2018) 8–14, <https://doi.org/10.1016/j.mten.2018.02.002>.

[28] A.G. Tamirat, W.N. Su, A.A. Dubale, C.J. Pan, H.M. Chen, D.W. Ayele, J.F. Lee, B.J. Hwang, Efficient photoelectrochemical water splitting using three dimensional urchin-like hematite nanostructure modified with reduced graphene oxide, *J. Power Sources* 287 (2015) 119–128, <https://doi.org/10.1016/j.jpowsour.2015.04.042>.

[29] S. Rai, A. Ikram, S. Sahai, S. Dass, R. Shrivastav, V.R. Satsangi, Photoactivity of MWCNTs modified α -Fe₂O₃ photoelectrode towards efficient solar water splitting, *Renew. Energy* 83 (2015) 447–454, <https://doi.org/10.1016/j.renene.2015.04.053>.

[30] X. Lv, K. Nie, H. Lan, X. Li, Y. Li, X. Sun, J. Zhong, S.T. Lee, Fe₂TiO₅-incorporated hematite with surface P-modification for high-efficiency solar water splitting, *Nano Energy* 32 (2017) 526–532, <https://doi.org/10.1016/j.nanoen.2017.01.001>.

[31] J. Deng, X. Lv, J. Liu, H. Zhang, K. Nie, C. Hong, J. Wang, X. Sun, J. Zhong, S.T. Lee, Thin-layer Fe₂TiO₅ on hematite for efficient solar water oxidation, *ACS Nano* 9 (2015) 5348–5356, <https://doi.org/10.1021/acsnano.5b0128>.

[32] C. Li, T. Wang, Z. Luo, S. Liu, J. Gong, Enhanced charge separation through ALD-modified Fe₂O₃/Fe₂TiO₅ nanorod heterojunction for photoelectrochemical water oxidation, *Small* (2016) 3415–3422, <https://doi.org/10.1002/smll.201600940>.

[33] J. Li, Y. Qiu, Z. Wei, Q. Lin, Q. Zhang, K. Yan, H. Chen, S. Xiao, Z. Fan, S. Yang, A three-dimensional hexagonal fluorine-doped tin oxide nanocone array: a superior light harvesting electrode for high performance photoelectrochemical water splitting, *Energy Environ. Sci.* 7 (2014) 3651–3658, <https://doi.org/10.1039/c4ee01581a>.

[34] M. Li, J. Deng, A. Pu, P. Zhang, H. Zhang, J. Gao, Y. Hao, J. Zhong, X. Sun, Hydrogen-treated hematite nanostructures with low onset potential for highly efficient solar water oxidation, *J. Mater. Chem. A* 2 (2014) 6727–6733, <https://doi.org/10.1039/c4ta00729h>.

[35] J. Zhong, H. Zhang, X. Sun, S.T. Lee, Synchrotron soft X-ray absorption spectroscopy study of carbon and silicon nanostructures for energy applications, *Adv. Mater.* 26 (2014) 7786–7806, <https://doi.org/10.1002/adma.201304507>.

[36] C. Zhu, M. Zhu, Y. Sun, Y. Zhou, H. Huang, Y. Lifshitz, S.T. Lee, J. Zhong, Y. Liu, Z. Kang, Defects induced efficient overall water splitting on a carbon-based metal-free photocatalyst, *Appl. Catal. B-Environ.* 237 (2018) 166–174, <https://doi.org/10.1016/j.apcatb.2018.05.071>.

[37] P. Zhang, T. Wang, X. Chang, L. Zhang, J. Gong, Synergistic cocatalytic effect of carbon nanodots and Co₃O₄ nanoclusters for the photoelectrochemical water oxidation on hematite, *Angew. Chem. Int. Ed.* 55 (2016) 5851–5855, <https://doi.org/10.1002/anie.201600918>.

[38] K. Feng, J. Zhong, B. Zhao, H. Zhang, L. Xu, X. Sun, S.T. Lee, Cu_xCo_{1-x}O nano-particles on graphene oxide as a synergistic catalyst for high-efficiency hydrolysis of ammonia-borane, *Angew. Chem. Int. Ed.* 55 (2016) 11950–11954, <https://doi.org/10.1002/anie.201604021>.

[39] J. Stöhr, *NEXAFS Spectroscopy*, Springer-Verlag, Berlin, 1992, pp. 114–160.

[40] M.A. Garakani, S. Abouali, B. Zhang, Z.L. Xu, J.Q. Huang, J.Q. Huang, E.K. Heidari, J.K. Kim, Controlled synthesis of cobalt carbonate/graphene composites with excellent supercapacitive and pseudocapacitive characteristics, *J. Mater. Chem. A* 3 (2015) 17827–17836, <https://doi.org/10.1039/c5ta02916c>.

[41] Y. Zhao, H. Zhang, H. Ji, W. Ma, C. Chen, J. Zhao, Pivotal role and regulation of proton transfer in water oxidation on hematite photoanodes, *J. Am. Chem. Soc.* 138 (2016) 2705–2711, <https://doi.org/10.1021/jacs.5b12069>.

[42] Y. Zhang, Z. Zhou, C. Chen, Y. Che, H. Ji, W. Ma, J. Zhang, D. Song, J. Zhao, Gradient FeOx(PO₄)_y layer on hematite photoanodes: novel structure for efficient light-driven water oxidation, *ACS Appl. Mater. Interfaces* 6 (2014) 12844–12851, <https://doi.org/10.1021/am502821d>.

[43] B. Klahr, S. Giménez, F. Fabregat-Santiago, J. Bisquert, T.W. Hamann, Photoelectrochemical and impedance spectroscopic investigation of water oxidation with "Co-Pi"-coated hematite electrodes, *J. Am. Chem. Soc.* 134 (2012) 16693–16700, <https://doi.org/10.1021/ja30642f>.